ChemPubSoc Europe

DOI: 10.1002/chem.201803821

CHEMISTRY A European Journal Full Paper

Magnetic Properties

Magnetization Blocking in $Fe_2^{III}Dy_2^{III}$ Molecular Magnets: Ab Initio Calculations and EPR Spectroscopy

Veacheslav Vieru,[a] Liviu Ungur,[a, e] Valeriu Cemortan,[a] Andrey Sukhanov,[b] Amer Baniodeh,[c] Christopher E. Anson,[c] Annie K. Powell,*[c, d] Violeta Voronkova,*[b] and Liviu F. Chibotaru*[a]

Abstract: The magnetism and magnetization blocking of a series of $[Fe_2Dy_2(OH)_2(teaH)_2(RC_6H_4COO)_6]$ complexes was investigated, in which $teaH_3$ = triethanolamine and R = *meta*-CN (**1**), *para*-CN (**2**), *meta*-CH_3 (**3**), *para*-NO_2 (**4**) and *para*-CH_3 (**5**), by combining ab initio calculations and EPR measurements. The results of broken-symmetry DFT calculations show that in all compounds the Fe–Fe exchange interaction is antiferromagnetic and stronger by far than the Fe–Dy and Dy–Dy interactions. As a result, the lowest two exchange doublets probed by EPR spectroscopy mostly originate from the Ising interaction of the dysprosium ions in all compounds. A correct quantitative description of the splitting of these two doublets requires, however, an explicit account of the Fe–Dy and Fe–Fe interactions. Due to the inversion symmetry of the complexes, the doublets under consideration are described by a collinear Ising exchange interaction. This picture is also supported by the EPR spectra, which could be simulated with parameters close to those extracted from the calculations. The magneto-structural analysis shows an increase of the antiferromagnetic Fe–Fe exchange interaction with increasing Fe-O-Fe angle and Fe–Fe distance. For the Dy–Fe interaction, the opposite tendency is observed, that is, a decrease of antiferromagnetic exchange coupling with increasing Dy-O-Fe angle and Dy–Fe distance. The transversal *g* factors extracted from the ab initio calculations have values in the range of 0.01–0.2, testifying to the lack of high axiality of the ground state of the dysprosium ions. This explains the lack/poor single-molecule magnetic behavior of this series of compounds at the investigated temperatures of a few Kelvin. Due to a very small gap (fractions of a wavenumber) between the ground and first-excited exchange doublet, relaxation takes place by magnetic moment reversal at individual dysprosium sites in the considered temperature domain.

Introduction

Since the discovery of the first single-molecule magnet (SMM),[1] there has been considerable interest in polynuclear transition-metal clusters due to their magnetization blocking properties. As such, they behave as tiny magnets but of the molecular origin, thus making them potential candidates for molecular spintronics, quantum computers, and high-density storage devices.[2–5] Although the first reported SMM, the Mn_{12} acetate complex, contains only transition-metal ions, subsequent incorporation of 4f elements has proved fruitful because these provide large unquenched orbital moments resulting in a large atomic total momentum *J*. This helps to fulfil the prerequisites for a good SMM, providing quantum tunneling of magnetization (QTM) can be controlled. A performant SMM should possess a high relaxation barrier of magnetization, high coercivity in the magnetic hysteresis loops, and a high blocking temperature. Until recently, the N_2^{3-} radical-bridged dilanthanide complex $[(\{(Me_3Si)_2N\}_2\{thf\}Tb^{III})_2(\mu\text{-}\eta^2\text{:}\eta^2\text{-}N_2)]$[6] showed the highest observed blocking temperature of 14 K amongst polynuclear compounds. However, more recently, the endohedral fullerene $Dy_2@C_{80}$ was shown to have a blocking temperature of 18 K[7] and $[K(crypt\text{-}222)][(Cp^{Me4H}{}_2Tb)_2(\mu\text{-}N_2^{\cdot})]$ a value of up to 20 K.[8]

Dedicated studies have established that a good strategy for the synthesis of performant SMMs would be the combination of strongly axial ions with fully isotropic ions through a strong exchange interaction.[9] A natural approach to achieve this is to

[a] Dr. V. Vieru, Prof. Dr. L. Ungur, V. Cemortan, Prof. Dr. L. F. Chibotaru
Theory of Nanomaterials Group, Katholieke Universiteit Leuven
Celestijnenlaan 200F, 3001 Leuven (Belgium)
E-mail: Liviu.Chibotaru@kuleuven.be

[b] Dr. A. Sukhanov, Dr. V. Voronkova
Zavoisky Physical-Technical Institute, FRC Kazan Scientific Center of RAS
Kazan (Russian Federation)
E-mail: vor18@yandex.ru

[c] Prof. Dr. A. Baniodeh, Dr. C. E. Anson, Prof. Dr. A. K. Powell
Institute of Inorganic Chemistry, Karlsruhe Institute of Technology
Engesserstrasse 15, 76131 Karlsruhe (Germany)
E-mail: Annie.Powell@kit.edu

[d] Prof. Dr. A. K. Powell
Institute of Nanotechnology, Karlsruhe Institute of Technology
Postfach 3640, 76021 Karlsruhe (Germany)

[e] Prof. Dr. L. Ungur
Department of Chemistry, National University of Singapore
Block S8 Level 3, 3 Science Drive 3, Singapore 117543 (Singapore)

Supporting information and the ORCID identification number(s) for the author(s) of this article can be found under: https://doi.org/10.1002/chem.201803821. Details of ab initio calculations, magnetization data, and EPR measurements.

piece together strongly anisotropic lanthanide ions, such as Dy^{III} and Tb^{III}, and fully isotropic transition-metals ions, such as Fe^{III} and Cr^{III}, resulting in a magnetization blocking barrier of the exchange type. For instance, in a series of Dy_2Cr_2 compounds, the quantum tunneling of magnetization (QTM) is suppressed due to a strong magnetic exchange interaction between Dy^{III} and Cr^{III} leading to a multilevel relaxation barrier.[10] In these systems, the height of the barrier can be associated with the strength of the exchange interaction between Dy^{III} and Cr^{III}. Generally, 3d metal ions can enhance the strength of the exchange interaction, the latter being rather weak in pure 4f compounds. A similar tendency to enhance the blocking properties through the interplay of isotropic ions with strongly axial metal ions has been observed in a series of $Ni^{II}Ln^{III}W^{V}$ heterotrimetallic complexes.[11]

Although this approach is promising, it is not easy to foresee a priori what systems will be good magnets. However, by combining experimental studies with ab initio calculations, we can gain in many cases the necessary insight. As a result of these studies, there is now a wide consensus that good SMM behavior is displayed by complexes with highly axial metal ions possessing very low transversal components of the ***g*** tensor of their ground doublet.[12,13] Therefore gaining an insight into the role of structural factors that can modulate the axiality of individual magnetic ions in polynuclear exchange-coupled complexes is of primary importance for the field. Such complexes have been investigated intensively with respect to the nearest-neighbor environment of the metal ions, and some systems for the role of distant substituents by using Mössbauer spectroscopy.[14–16] However, studies on the effect of distant ligand substitution by means of ab initio calculations are still scarce. Here, we fill this gap by reporting a combined study of ab initio calculations and electron paramagnetic resonance (EPR) spectroscopic analysis of a series of $[Fe_2Dy_2(OH)_2(teaH)_2(RC_6H_4COO)_6]$ compounds, in which $teaH_3$ = triethanolamine and R = *meta*-CN (**1**), *para*-CN (**2**), *meta*-methyl (**3**), *para*-NO_2 (**4**), and *para*-methyl (**5**) (Figure 1). These complexes were synthesized and characterized earlier[14,15] and here we present only the results of their EPR and ab initio analysis. We analyze the effect of different substituents on the magnetic properties of these compounds and explain the observed magnetization blocking behavior.

Experimental Section

Crystal structures: The crystal structures of **1**–**5** have been reported previously[14,15] and the structures deposited at the CCDC (926560 (**1**), 866243 (**2**), 926561 (**3**), 866242 (**4**), and 866240 (**5**)).

Magnetic measurements: The temperature dependence of the magnetic susceptibility of powdered samples of **1**–**3** and **5** was measured in the 2–300 K temperature range and have been reported earlier.[15] The isothermal magnetization measurements for **1**–**5** were carried out at 2, 3, and 5 K between 0 and 7 T.

EPR measurements: X-band EPR spectra of polycrystalline samples of **1**, **2**, **4**, and **5** were recorded over the temperature range 4–30 K on a Bruker EMX/plus spectrometer in both perpendicular and parallel modes and on a Bruker ELEXSYS E 580 spectrometer in the perpendicular mode at temperatures down to 2.3 K. Q-band measurements were carried out for these four compounds on a Bruker ELEXSYS E 580 spectrometer over the temperature range 5–30 K. The measurements in W-band at 4.2 K for **5** were performed on a Bruker ELEXSYS E 680 spectrometer.

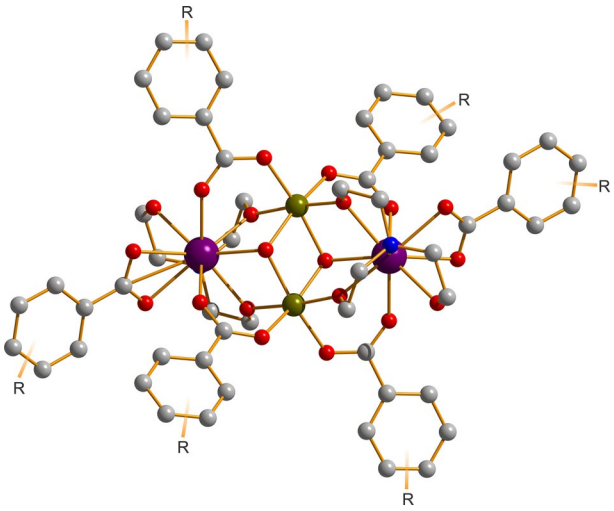

Figure 1. Structures of **1**–**5**. Color scheme: Pink (Dy), green (Fe), gray (C), red (O). R = *meta*-CN (**1**), *para*-CN (**2**), *meta*-methyl (**3**), *para*-NO_2 (**4**), and *para*-methyl (**5**). Hydrogen atoms are not shown for clarity.

Computational details: The unfeasibility of a full ab initio calculation with all the magnetic centers included in the same calculation required fragment ab initio calculations to be performed on only one magnetic center, which allowed us to determine the local properties. Once we had calculated the local properties, the exchange interaction was considered within the Lines model.[17,18] Fragment ab initio calculations were performed by using the Molcas 8.0 program package.[18–20] First, a complete active space self-consistent field (CASSCF) calculation was carried out[21] to calculate the spin-free states. Secondly, the obtained spin-free states were mixed by spin–orbit coupling within the restricted active space state interaction (SO-RASSI) approach.[22] Based on the obtained spin–orbital states, local magnetic properties were calculated by using the SINGLE ANISO program.[23] The exchange interaction between the magnetic centers was then computed within the POLY ANISO program,[24] which uses the previously calculated local properties derived from the SINGLE ANISO module.

Due to the presence of the inversion center in the investigated compounds, it suffices to calculate only one dysprosium center per compound. Each dysprosium center was calculated by keeping the experimentally determined positions of all atoms and replacing the neighboring magnetic centers by diamagnetic ions, for example, Dy^{III} was replaced by Lu^{III} and Fe^{III} by Zn^{II}. Fe^{III} centers were not calculated ab initio but were considered isotropic. Two sets of basis sets were employed (see Table S1 in the Supporting Information for details). The Cholesky decomposition threshold was set to 5×10^{-8} to save disk space. The active space at the CASSCF level consisted of nine electrons in seven 4f-type orbitals. All sextet, quartet, and doublet states were calculated within CASSCF, but only 21 sextet states (all), 128 quartet states (out of 224), and 130 doublet states (out of 490) were mixed by spin–orbit coupling due to the limitations of disk space.

Broken-symmetry density functional theory (BS-DFT) calculations were carried out by using the ORCA 3.0.0 program.[25,26] The calculations were performed by using the Douglas–Kroll–Hess Hamilto-

nian, the SVP basis set for all atoms,[27,28] and the B3LYP functional as implemented in ORCA.

Results and Discussion

Magnetic properties

The magnetic behavior of compounds **1**–**5** was investigated in the temperature range of 2–300 K. The χT versus T curves are shown in Figure 2 and the M versus H curves are presented in Figure S1 in the Supporting Information. For all five compounds, the room-temperature values of the χT product are close to those expected for two Dy^{III} and two Fe^{III} ions that are magnetically isolated. For each compound, the χT product slowly decreases with temperature and then drops quickly below 25 K. The decrease in χT in the high-temperature domain is associated with the depopulation of the excited crystal field (CF) levels of Dy^{III}, whereas the rapid decrease at lower temperature is related to the depopulation of the exchange coupling states involving Fe^{III} ions (see below). The magnetization plots show a rapid increase below 2 T and a slower increase at higher fields without reaching saturation at 7 T, which is explained by the existence of low-lying excited exchange states resulting from Fe–Dy and Fe–Fe interactions.

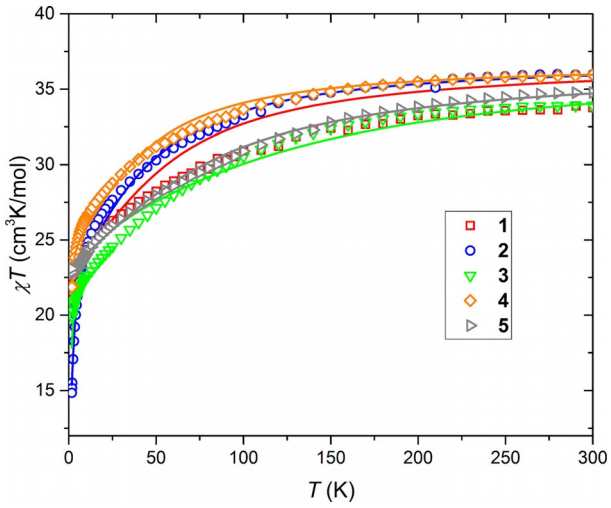

Figure 2. Experimental (symbols) and calculated (lines) molar magnetic susceptibilities for **1**–**5**. Experimental curves for **2** and **5** are scaled up by 3.5 and 8.5 %, respectively (see text for details).

Ab initio calculations

Ab initio calculations for the dysprosium centers in 1–5

The lowest calculated local spin–orbit levels of the dysprosium centers originating from $J=15/2$ in complexes **1**–**5** are shown in Table 1. All shown levels are double-degenerate Kramers doublets because Dy^{III} has an odd number of electrons.[29] The data in Table 1 show that the ground Kramers doublet (KD) of the dysprosium ions in each compound is well separated from the excited states, which means that the low-lying exchange energy levels will originate mainly from these. The transversal components of the ground ***g*** tensor (g_x and g_y, Table 1) are significantly smaller than the axial component g_z, which indicates an Ising type of exchange interaction. Although complexes **1**–**5** are isostructural, their transversal components differ slightly. This can be explained by the different distribution of electron density in the benzene ring, which induces small differences in the crystal field. The orientations of the main magnetic axes of the dysprosium centers in **1** are shown in Figure 3 top, and they are parallel to each other due to the presence of the inversion center in the complexes under study. The magnetic axes in **2**–**5** have similar orientations (Figure 3 bottom). Their angles θ with the Dy–Dy axis are given in Table 5.

Table 1. Energies of the lowest KDs of dysprosium centers and the g factors of the ground KD in **1**–**5**.

	Energy [cm^{-1}]				
	1	**2**	**3**	**4**	**5**
	0	0	0	0	0
	86	115	106	106	87
	122	180	188	148	126
	150	189	228	177	164
	170	241	279	215	193
	210	266	311	254	207
	295	332	385	332	273
	386	479	459	446	434
	g factors of the ground KDs				
g_x	0.13	0.052	0.012	0.062	0.12
g_y	0.22	0.088	0.026	0.086	0.20
g_z	19.20	19.50	19.66	19.43	19.19

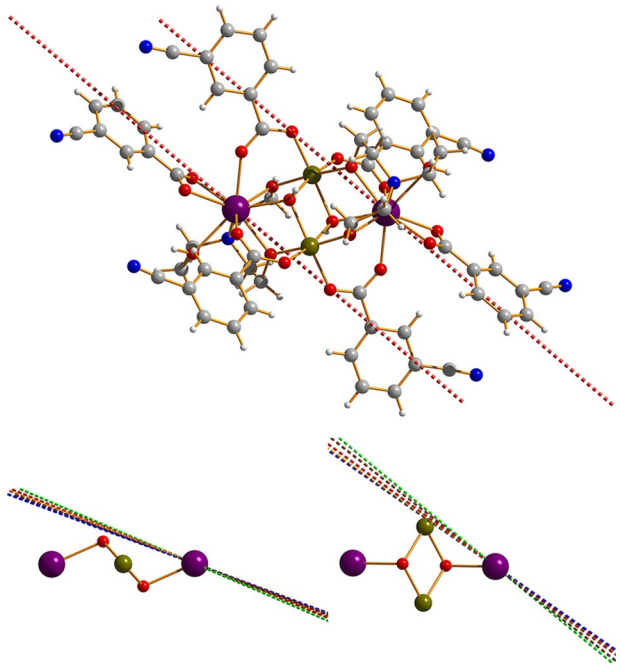

Figure 3. Top) Orientations of the local main magnetic axes of the dysprosium ions in compound **1**. Bottom) Orientations of the local main magnetic axes of the dysprosium ions in **1** (red), **2** (brown), **3** (green), **4** (orange), and **5** (blue) viewed from two perspectives.

Exchange interaction and magnetization blocking in 1–5

The investigated compounds consist of four magnetic centers related pairwise by an inversion symmetry. Because the wavefunctions of the KDs on the dysprosium ions are complex and multideterminantal due to first-order spin–orbit coupling effects, the BS-DFT approach cannot be straightforwardly applied to describe the exchange interaction. To circumvent this problem, we replaced Dy^{III} with Gd^{III}, which can be well described by a single-determinant wavefunction, and kept the positions of all the other atoms in the corresponding complexes intact.[10] We computed the exchange coupling parameters for all the magnetic pairs by using a generalized spin-projection method,[30] which is an extended algorithm of Yamaguchi et al.'s approach.[31] Then we rescaled the obtained *J*(Gd–Gd) parameters from the spin 7/2 of Gd^{III} to the spin 5/2 of Dy^{III} by multiplying the former by 49/25.[10] The same rescaling scheme was applied to the treatment of Gd–Fe pairs, in this case, the rescaling factor was 7/5. Such a rescaling procedure provides a satisfactory estimation of the exchange parameters used for the Lines description of the Dy–Dy and Dy–Fe anisotropic exchange interaction described below.[12,18] Despite its simplicity, this approach proved to be reliable for the description of the magnetic properties of a series of Dy_2Cr_2[10] and Ln_2[32] compounds. The calculated exchange parameters (Figure 4) are presented in Table 2 and show that in all compounds there is an antiferromagnetic interaction between iron centers. The antiferromagnetic interaction between iron centers can be explained by the direct overlap of their magnetic orbitals (Figure 5). As we can see in Figure 5, the magnetic orbitals of one iron ion have tails on the second iron ion and on the bridging oxygen atoms connecting them, which results in their efficient overlap. This implies that the antiferromagnetic kinetic mechanism is dominant in these complexes.

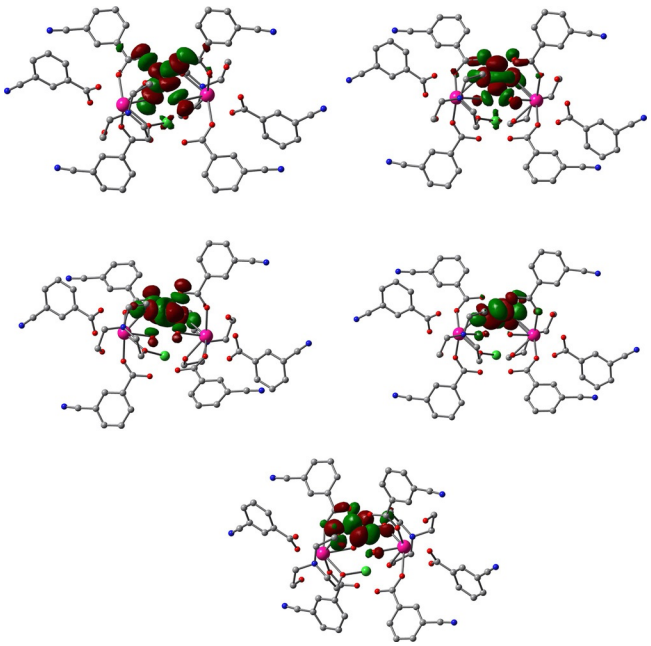

Figure 5. Magnetic orbitals on one of the iron centers in **1** obtained from DFT calculations. Similar orbitals were obtained for **2**–**5**.

A similar situation occurs for the gadolinium and iron centers. The magnetic orbitals of the gadolinium centers have tails on the bridging oxygen atoms connecting them with the iron atoms, and the magnetic orbitals of the iron centers have tails on the oxygen bridging atoms as well (Figure 6). Therefore, these pairs of magnetic orbitals show a direct overlap too and the kinetic mechanism is again responsible for the antiferromagnetic interaction between these magnetic centers.

Analyzing the bond distances between the iron ions and the angle Fe-O-Fe, in which the oxygen is a bridging oxygen, one observes the following trend (Figure 7): With an increase in the Fe-O-Fe angle and Fe–Fe distance the antiferromagnetic exchange interaction increases. This trend is similar to that observed in a series of $[Fe_6]$ compounds.[33] In the case of Dy–Fe interactions, an opposite trend is observed (Figures 8 and 9): With an increase in the angle Dy-O-Fe angle and Dy–Fe distance the strength of the antiferromagnetic interaction decreases. The greater deviation of the calculated points from a smooth line in Figures 8 and 9 compared with in Figure 7 is explained by a much smaller Dy–Fe exchange interaction compared with Fe–Fe, and the accompanying stronger effect of the convergence error on its value. Moreover, the exchange interaction between iron centers is through only two bridging oxygen atoms and the strength of the exchange interaction depends mainly on the Fe-O-Fe angle and the distance between them. On the other hand, for the Dy–Fe pairs, there are more possible paths for the exchange interaction (Figure 1), which is why in this case there is a stronger deviation from the smooth line (Figures 8 and 9).

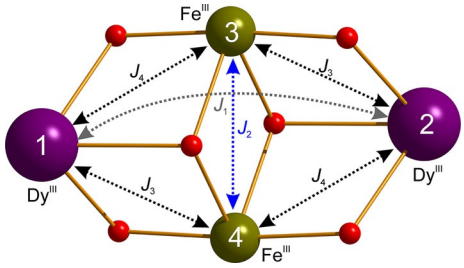

Figure 4. Parameters used for the simulation of exchange interactions. Note that J_3 and J_4 cannot be constrained to be equal, as the molecular structure as a whole (and particularly the coordination geometry around Dy) is not consistent with any mirror plane through the dysprosium and triply-bridging oxygen atoms.

Table 2. BS-DFT versus fitted exchange coupling parameters of **1**–**5**.[a]

	J_1 [cm^{-1}]		J_2 [cm^{-1}]		J_3 [cm^{-1}]		J_4 [cm^{-1}]	
	BS-DFT	Fitted	BS-DFT	Fitted	BS-DFT	Fitted	BS-DFT	Fitted
1	−0.024	−0.024	−8.6	−8.6	−0.31	−0.31	−0.17	−0.17
2	−0.0067	−0.0070	−5.7	−5.7	−0.12	−0.13	−0.090	−0.090
3	−0.011	−0.015	−8.2	−21.0	−0.21	−0.30	0.046	−0.010
4	0	0	−6.3	−5.0	−0.088	−0.0050	−0.11	−0.0050
5	−0.011	−0.010	−8.8	−14.0	−0.26	−0.26	−0.27	−0.27

[a] Better *J* values for **3** and **5** are provided in Table 3 (see text for details).

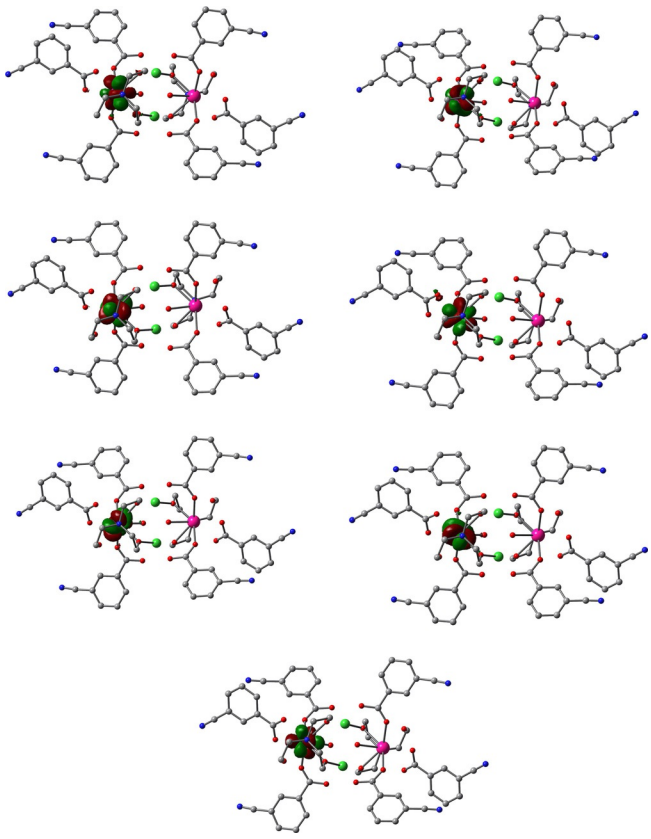

Figure 6. Magnetic orbitals on one of the gadolinium centers in **1** obtained from DFT calculations. Similar orbitals were obtained for **2**–**5**.

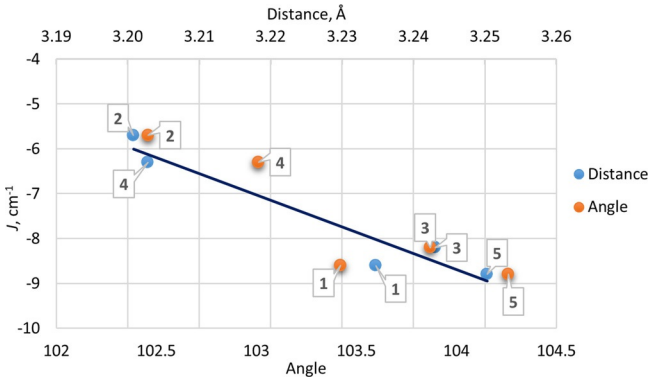

Figure 7. Dependence of the BS-DFT Heisenberg exchange parameter *J*(Fe–Fe) on the Fe-O-Fe angle and Fe–Fe distance in **1**–**5**.

The magnetic properties of the investigated complexes were calculated by using the module POLY ANISO of the Molcas package.[19] Because the ground KDs of the dysprosium ions are well separated from the excited states, we included only them in the exchange interaction. The iron ions were considered isotropic with a *g* factor of 2.0. The exchange interactions were treated within the Lines model.[17] This approach allows for an approximate treatment of an anisotropic exchange interaction by using only one fitting parameter per exchange pair and is well justified for strongly axial and isotropic magnetic ions.[9,12] The employed Lines exchange Hamiltonian is given by Equation (1)

Figure 8. Dependence of the BS-DFT Lines exchange parameter *J*(Dy1–Fe3) on the Dy1-O-Fe3 angle and Dy1–Fe3 distance in **1**–**5**.

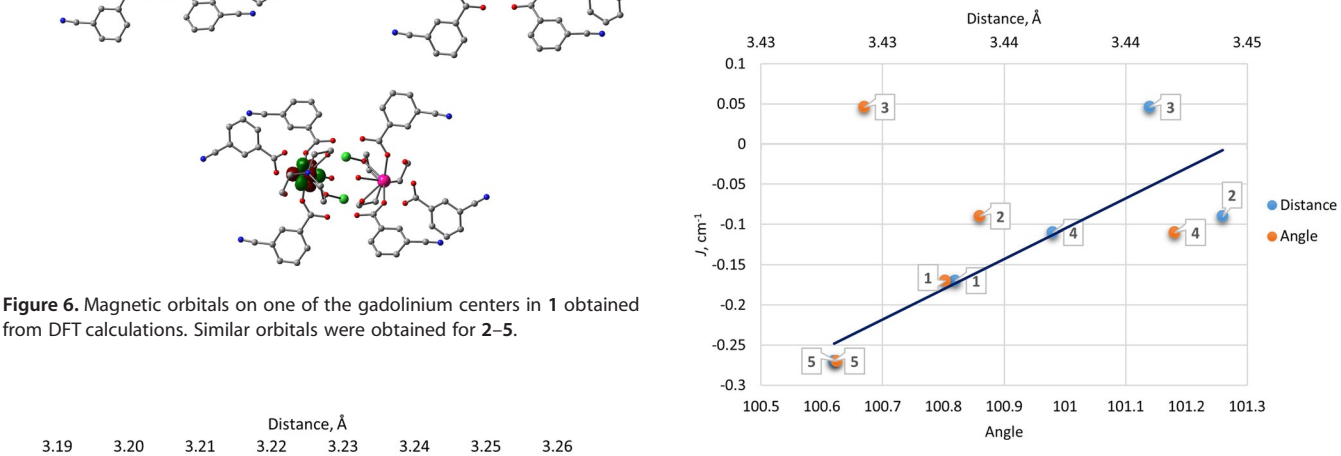

Figure 9. Dependence of the BS-DFT Lines exchange parameter[17] *J*(Dy1–Fe4) on the Dy1-O-Fe4 angle and Dy1–Fe4 distance in **1**–**5**.

$$\hat{H} = -J_1\vec{S}_{Dy1}\vec{S}_{Dy2} - J_2\vec{S}_{Fe3}\vec{S}_{Fe4} - J_3(\vec{S}_{Dy2}\vec{S}_{Fe3} + \vec{S}_{Dy1}\vec{S}_{Fe4}) - J_4(\vec{S}_{Dy1}\vec{S}_{Fe3} + \vec{S}_{Dy2}\vec{S}_{Fe4}) \quad (1)$$

in which $S_{Dy} = 5/2$ and $S_{Fe} = 5/2$ and the exchange parameters are taken from Table 2.

The best description of magnetic susceptibility (Figure 2) is given by the parameters shown in Table 2. Although the agreement of $\chi T(T)$ with the experiment looks good, the fitted exchange parameters between the iron centers in **3** and **5** seem too large. Considering that all the compounds are isostructural and BS-DFT predicts a similar strength of the Fe–Fe interaction for the entire series, we repeated the fitting by taking the BS-DFT as a basis and also allowing for a small rescaling of the experimental data (Figure 10). By doing so, we found another set of fitted Lines parameters (Table 3) that are in line with the BS-DFT values. A small rescaling of the experimental data is in principle justified given the possible experimental errors due

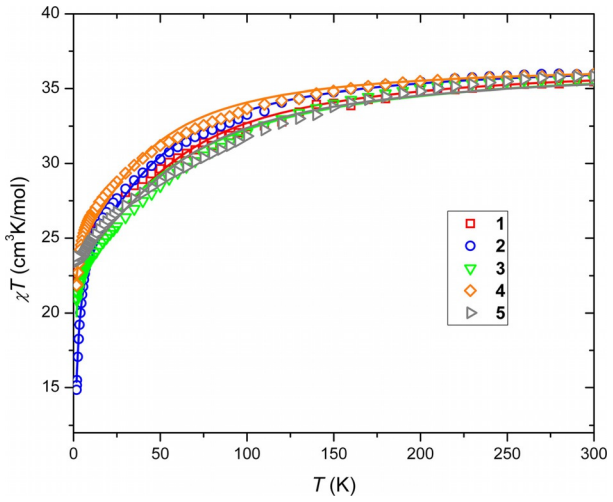

Figure 10. Experimental (symbols) and calculated (lines) molar magnetic susceptibilities for **1**–**5**. The calculations were performed with the Lines exchange parameters from Table 2 for **1**, **2**, and **4** and from Table 3 for **3** and **5**. The experimental curves are scaled up by 5, 3.5, 5, 8.5, and 3% for compounds **1**, **2**, **3**, **4**, and **5**, respectively (see the text).

Table 3. Refitted exchange coupling parameters in **3** and **5**.[a]

Interaction	3	5
J_1 [cm^{-1}]	−0.020	0
J_2 [cm^{-1}]	−10.0	−9.5
J_3 [cm^{-1}]	−0.17	−0.20
J_4 [cm^{-1}]	−0.10	−0.20

[a] See the text for details.

to the absorption of solvent molecules or mass error (of course, we do not exclude calculation errors too). The validity of this approach is also confirmed by the good agreement of experimental magnetization curves and those calculated by using the parameters from Tables 2 and 3 (see Figure S4 in the Supporting Information).

The calculated low-lying exchange spectra of **1**–**5** are presented in Table 4. Although all the complexes have an even number of electrons, and degeneracy of the levels is not expected by symmetry, we see that the exchange energy levels are grouped into almost degenerate doublets. The first-excited exchange doublet is placed quite close to the ground doublet, the energy gap varying from 0.04 to 0.47 cm^{-1}. This is a consequence of the weak values of the exchange and dipolar interactions between the dysprosium ions due to the relatively large Dy–Dy distance (Table 5).

As the data in Tables 2 and 3 show, the magnetic ions possess conflicting exchange interactions (Figure 4), which can give rise to frustration.[32,34] However, due to the dominant exchange interaction between the iron centers, the lowest two exchange doublets originate mainly from the collinear Ising exchange interaction between the dysprosium ions. Nevertheless, the exchange interaction between the dysprosium and iron ions still influences the energy of the low-lying exchange states (see below).

Table 4. Energies of the low-lying exchange spectra containing dipolar and exchange interactions in **1**–**5** and the g_z factors of the ground and first-excited doublets.

Energy [cm^{-1}]				
1	**2**	**3**	**4**	**5**
0	0	0	0	0
4.42×10^{-15}	5.79×10^{-6}	3.31×10^{-7}	1.49×10^{-5}	6.4×10^{-4}
0.0581	0.420	0.469	0.179	0.0404
0.0584	0.420	0.469	0.179	0.0412
7.60	5.50	9.75	4.73	8.623
7.60	5.50	9.75	4.73	8.624
8.47	5.94	10.15	5.01	9.558
8.47	5.94	10.15	5.01	9.560
8.48	6.09	10.28	5.15	9.586
8.48	6.09	10.28	5.15	9.592
8.74	6.21	10.57	5.25	9.623
8.74	6.21	10.57	5.25	9.627
9.09	6.67	11.00	5.82	10.294
9.09	6.67	11.00	5.82	10.298
9.64	6.90	11.08	6.06	10.310
9.64	6.90	11.08	6.06	10.314
		g_z		
0	0	0	0	38.09
38.33	38.99	39.32	38.87	0

Table 5. Magnetic interactions between Dy^{III} corresponding to pseudospin $\tilde{s} = 1/2$ of the ground KDs on the dysprosium sites in **1**-**5**, the angle θ between their main magnetic axis on dysprosium and the Dy–Dy axis, and φ, the smallest of the two angles between the dysprosium main magnetic axis and the Dy–Fe axis.

Compound	1	2	3	4	5
J_{Ising} [cm^{-1}] [Eq. (3)]	−0.60	−0.18	−0.50	0	0
J_{dip} [cm^{-1}]	0.57	0.53	0.48	0.61	0.65
J_{total} [cm^{-1}] [Eq. (4)]	−0.03	0.35	−0.02	0.61	0.65
θ [°]	39.3	40.5	42.4	38.4	37.5
φ [°]	20.0	19.7	21.6	19.5	18.4

The data in Tables 2 and 3 show that the exchange interactions between all magnetic centers are antiferromagnetic. On the other hand, the exchange interactions between the gadolinium and iron ions in $[Fe_2Gd_2(OH)_2(teaH)_2(C_6H_5COO)_6]$ (which has an isostructural core with **1**–**5**) are weakly ferromagnetic.[16] For the sake of completeness, we tried to fit the magnetic susceptibility data of **1**–**5** with the ferromagnetic Dy–Fe interaction, which yielded a poorer agreement with experiment. In particular, the energy gap between the lowest two doublets is strongly modified. For instance, if one changes the sign of the *J*(Dy–Fe) parameters for **1** in Table 2 to positive, the gap changes from 0.058 to 0.77 cm^{-1}. This shows that this exchange interaction can only be antiferromagnetic. On the other hand, given that the values of *J*(Dy–Fe) are small, even some slight distortions in the Ln_2Fe_2 core can change the sign of this interaction, which is the case for the Gd_2Fe_2 complex.

The general form of the exchange interaction between two pseudospins $\tilde{s} = 1/2$, which corresponds to the ground KD on the dysprosium sites, is given by Equation (2)

$$\hat{H}_{exch} = \vec{\tilde{s}}_1 \boldsymbol{J} \vec{\tilde{s}}_2 \qquad (2)$$

in which $\boldsymbol{J}$ is the 3×3 exchange matrix, the nine elements of which can be parametrized with one isotropic parameter, five symmetric anisotropic parameters, and three antisymmetric exchange parameters (Dzyaloshinsky–Moriya).[35–37] Because of the presence of the inversion center, the antisymmetric parameters are zero. As a result, the matrix $\boldsymbol{J}$ becomes symmetric ($J_{\alpha\beta}=J_{\beta\alpha}$, $\alpha=x, y, z$), that is, containing six independent matrix elements. Due to the high axiality of the dysprosium ions, the matrix $\boldsymbol{J}$ rewritten in coordinate system coinciding with the main magnetic axes on the dysprosium sites will contain one dominant parameter J_{zz}, in which z corresponds to the largest g factor (the last line in Table 1). Then the exchange Hamiltonian reduces to a collinear Ising form[38] ($J_{\text{Ising}}\equiv J_{zz}$), given by Equation (3).

$$\widehat{H}_{\text{Ising}} = -J_{\text{Ising}}\tilde{S}_{1,z}\tilde{S}_{2,z} \quad (3)$$

The obtained Lines parameters J_i in Table 2 are easily projected onto the Ising parameters from Equation (3) by multiplying them by a factor of 25 (Table 5). To this interaction, one should add also the dipolar interaction, which has a similar collinear Ising form [Eq. (3)], due to the high axiality of the dysprosium sites. Having obtained the g factors and the main magnetic axes on the dysprosium sites, their dipolar (dip) interaction is calculated straightforwardly,[12,35] with the J_{dip} parameters given in Table 5. As a result, the total interaction between dysprosium sites is described by Equation (4).

$$J_{\text{total}} = J_{\text{Ising}} + J_{\text{dip}} \quad (4)$$

As the data in Table 5 show, the exchange Ising and dipolar interactions between dysprosium ions are weak and of opposite signs. The data also show that the dipolar interaction decreases with increasing angle between the dysprosium main magnetic axis and the Dy–Dy axis (Figure 3). Given the strong antiferromagnetic interaction between the iron centers, one would expect the presence of iron ions not to influence the low-lying energy spectrum. In this case, the obtained gap between the lowest two exchange doublets (Table 4) would be as large as $J_{\text{total}}/2$, in which J_{total} is the total interaction (exchange + dipolar) between the dysprosium ions only (Table 5). However, the data in Table 4 show that this gap is very different from that calculated as $J_{\text{total}}/2$. Therefore, despite being strongly antiferromagnetic, the exchange interaction between the iron ions and Dy–Fe still has a significant impact on the magnitude of the splitting of the lowest two exchange doublets. Moreover, it also influences the nature of the ground doublet, being able to change it from magnetic ($J_{\text{total}}>0$) to nonmagnetic ($J_{\text{total}}<0$) and vice versa. Thus, the data in Table 4 show that complexes **1**–**4** are nonmagnetic in their ground state, whereas **5** is magnetic, although from the signs of the J_{total} values in Table 5, one should conclude that **2** and **4** are magnetic.

By analyzing the obtained exchange spectra, we can see that the energy of the third exchange doublet (Table 4, Figure 11) scales with the strength of the exchange interaction between iron centers. Because the third doublet corresponds to the decoupling of iron spins (Figure 11), there is an increase in the total magnetic moment, which can be inferred from the $\chi T(T)$ plots (Figure 2). For compound **4** the Fe–Fe interaction is the weakest and, as a result, the effective decoupling of the iron magnetic moments occurs at a lower temperature, and therefore the $\chi T(T)$ curve lies higher than those of the other compounds (Figure 2). For the latter, the same trend is observed, that is, the position of the $\chi T(T)$ plot matches the strength of the corresponding Fe–Fe exchange interaction.

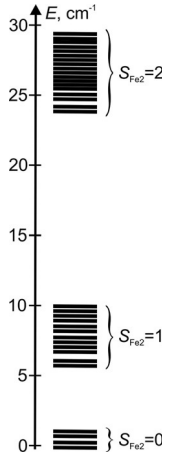

Figure 11. Low-lying exchange multiplets in **1**. S_{Fe} is the total spin of the Fe_2 dimer. The exchange spectra of **2**–**5** show a similar structure.

The fact that the first-excited exchange doublet is very close to the ground doublet explains the observed poor SMM behavior[15] in these compounds at the investigated temperatures ($T>1$ K). The situation is very close to frustrated systems in which, due to the quasi-degeneracy of the low-lying doublets, the relaxation proceeds by spin reversal of individual lanthanide sites.[32] However, individual dysprosium ions cannot block the magnetization, because in all the investigated compounds they are far from being strongly axial, $g_x, g_y \approx 0.01$–0.2. Moreover, the neighboring dysprosium ions are sources of oscillating magnetic (exchange) field, thereby enhancing further the quantum tunneling of the magnetic moment at a given dysprosium site.

We previously suggested that the differences in the ^{57}Fe Mössbauer spectra of some of these compounds could be explained in terms of differing orientations of their dysprosium magnetic axes, with the iron nuclei lying closer to their respective dysprosium axis ("searchlight beam") experiencing a greater contribution to their hyperfine fields from the dysprosium.[14] Figure 3 bottom now provides quantitative confirmation of our previous schematic diagram (see Figure 3 in Ref. [14]). The angles φ between the dysprosium axes and the corresponding Dy–Fe vectors are thus important in this respect and are listed here in Table 5.

EPR spectroscopy

The EPR spectra of the investigated compounds were recorded as described in the Experimental Section and simulated by using the EasySpin software.[39] Details of the recorded spectra are given in the Supporting Information. We discuss below the simulated data for **1**, **4**, and **5** together with the parameters extracted from the magnetic data and ab initio calculations. The EPR signals are observed at weak fields similarly to the signal observed for the $[Fe_2Dy_2(\mu_3\text{-}OH)_2(teaH)_2(O_2CPh)_6]$ compound, which has an isostructural core with **1**–**5**.[16]

Ab initio calculations have shown that the low-lying energy levels in these systems consist of two Ising doublets, which are separated from the excited states by 5–10 cm^{-1} (Table 4). The temperature dependence of the EPR signal intensity within the

temperature range of 4–20 K indicates that the spectra are due to transitions only in these low-lying doublets. When the ground exchange doublet is magnetic ($g_z \neq 0$), as in complex **5**, its states can be represented as $\psi_1 = \frac{1}{\sqrt{2}}(|\uparrow\uparrow\rangle + |\downarrow\downarrow\rangle)$ and $\psi_2 = \frac{1}{\sqrt{2}}(|\uparrow\uparrow\rangle - |\downarrow\downarrow\rangle)$ (Figure 12). The states of the excited doublet are then $\psi_3 = \frac{1}{\sqrt{2}}(|\uparrow\downarrow\rangle + |\downarrow\uparrow\rangle)$ and $\psi_4 = \frac{1}{\sqrt{2}}(|\uparrow\downarrow\rangle - |\downarrow\uparrow\rangle)$. In these equations the arrows represent the direction of the magnetic moments on the dysprosium sites along their main magnetic axis. When a field is applied, the ground doublet experiences Zeeman splitting much larger than the gap between the doublets and the two components of the magnetic doublet become $\psi_g = |\uparrow\uparrow\rangle$ and $\psi_e = |\downarrow\downarrow\rangle$ (Figure 12). On the other hand, the excited doublet does not split due to its nonmagnetic nature. From Figure 12 it is clear that the EPR signals will appear due to $\psi_g \leftrightarrow \psi_3$ and $\psi_e \leftrightarrow \psi_3$ transitions. The magnetic dipole matrix element connecting ψ_g, ψ_e, and ψ_4 is zero and transitions can occur only between the ψ_g and ψ_3 states and between the ψ_3 and ψ_e states with the matrix elements $M_{g,3} = \langle\psi_g|M_{x,y}|\psi_3\rangle$ and $M_{3,e} = \langle\psi_3|M_{x,y}|\psi_e\rangle$, respectively. The intensities of the transitions are proportional to the square of this matrix element, $I\left(\vec{H}_1\right) \propto \left|(M_x)_{i,j}\right|^2 \cos^2\varphi_x + \left|(M_y)_{i,j}\right|^2 \cos^2\varphi_y$, in which φ_x and φ_y are the angles between the applied microwave field H_1 (which is perpendicular to the applied field H) and the x and y axes perpendicular to the anisotropy axis (z) on the dysprosium sites. Due to the similar intensities of the $\psi_g \leftrightarrow \psi_3$ and $\psi_e \leftrightarrow \psi_3$ transitions given by the above expression and a very small splitting between the ground and first-excited doublets (resulting in their similar populations at the investigated temperatures), the two signals overlap and only one peak is observed in the EPR spectra of these complexes. For compounds **1**–**4**, the order of the levels is the opposite, but this does not affect the shape of the EPR spectra. In general, the signals corresponding to the z, x, and y principal axes of the ***g*** tensor should be observed in the EPR spectra of polycrystalline samples. For compounds **1**–**5**, due to small values of g_x and g_y of around 0.01–0.2, only the signals of molecules with z axes oriented along the magnetic field are seen in the spectra. The small values of g_x and g_y also explain the low intensity of signals corresponding to the z axes. A "forbidden" $\psi_3 \leftrightarrow \psi_4$ transition, the intensity of which increases with the deviation of the interaction symmetry from the axial symmetry can also be observed in the spectra of polycrystalline samples.

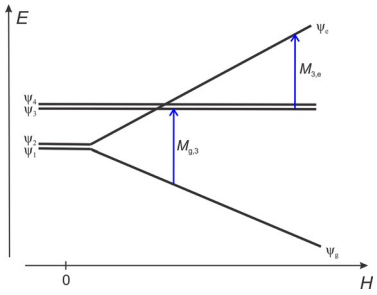

Figure 12. Schematic representation of the Zeeman splitting of the two lowest exchange doublets in applied field H along g_z. The EPR transitions are shown by blue arrows.

The total interaction $-J^*_{Ising}\tilde{S}_{1,z}\tilde{S}_{2,z}$ describing effectively these two Ising doublets, with exchange and dipolar contributions to their splitting from Fe–Dy and Fe–Fe interactions, is incorporated into the ab initio derived energy gap ΔE (Table 4), which defines the Ising parameter $J^*_{Ising} = 2\Delta E$.

The best agreement between the experimental and simulated EPR spectra using ab initio parameters derived in the previous section is obtained for complex **5** (Figure 13). These parameters, $g_x = 0.12$, $g_y = 0.20$, $g_z = 19.19$, and $J^*_{Ising} = 0.08\ cm^{-1}$ which corresponds to $\Delta E = 0.04\ cm^{-1}$ (Tables 1 and 4), were used in combination with the Hamiltonian similar to Equation (3).

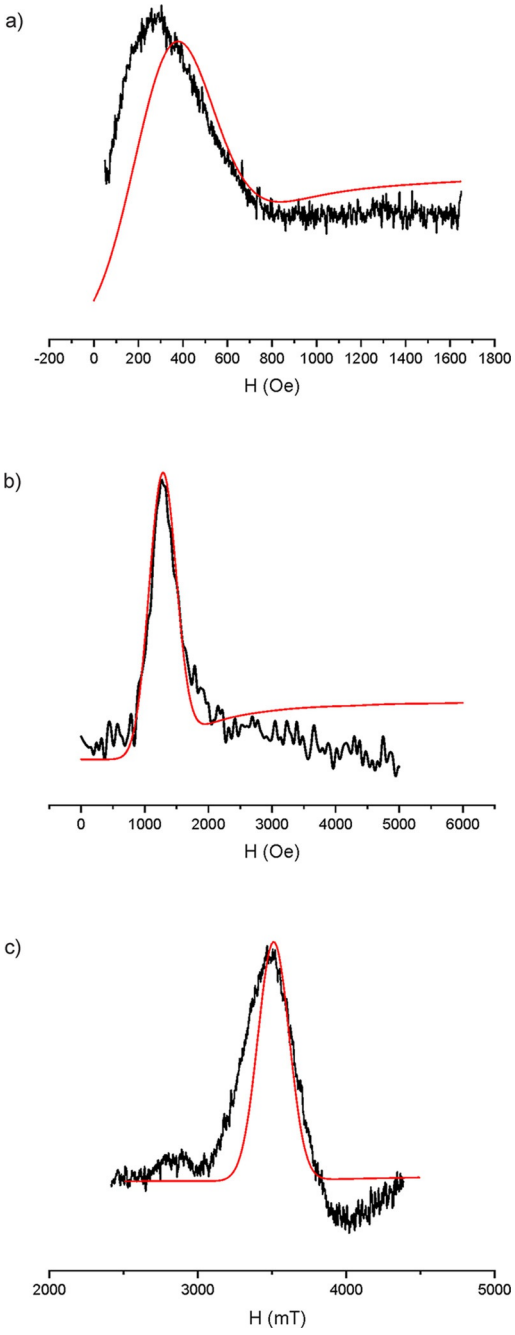

Figure 13. Experimental (black) and simulated (red) EPR spectra of **5**: (a) X-, (b) Q-, and (c) W-band spectra.

For compound **4**, it was possible to obtain a good agreement between the measured and simulated Q- and X-band EPR spectra (Figure 14) by allowing a small deviation from the Ising interaction by introducing also the parameter $J^*_{yy} = -0.013\ cm^{-1}$ in Equation similar to (2) and the parameter $J^*_{zz} = -0.27\ cm^{-1}$, which is slightly different from the value derived from Table 4, $J^*_{Ising} = -0.36\ cm^{-1}$. The values of the transversal g factors have little effect on the EPR spectrum and the g values from the ab initio calculations (Table 1) were used in the simulation.

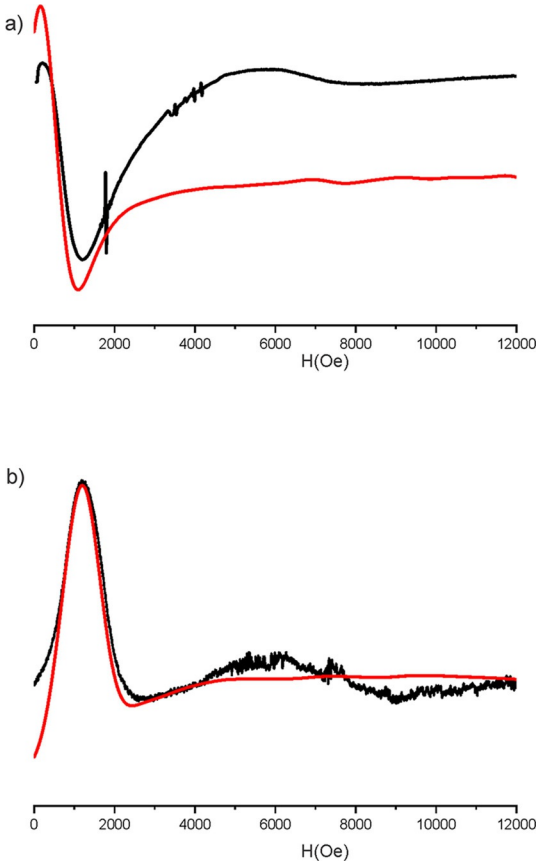

Figure 14. Experimental (black) and simulated (red) EPR spectra of **4** recorded at $T = 5$ K: (a) X- and (b) Q-band spectra.

For compound **1**, the X-band EPR spectrum (Figure 15) could be described satisfactorily with the ab initio parameters $J^*_{Ising} = -0.116\ cm^{-1}$ (derived from Table 4), by adding, as in the case of compound **4**, a J^*_{yy} term to the basic Ising Hamiltonian in Equation similar to (3), the value of which is relatively small ($J^*_{yy} = 0.016\ cm^{-1}$). The transversal components of the $\boldsymbol{g}$ tensor also have little effect on the EPR spectrum and the g values from the ab initio calculations (Table 1) were used in the simulation.

In the case of compound **2**, Figure S9 in the Supporting Information shows that the EPR signal in the Q-band spectrum is shifted to a much stronger magnetic field, which makes it impossible to simulate with the ab initio value of $g_z \approx 19$ (Table 1). The right position of the signal is only obtained for

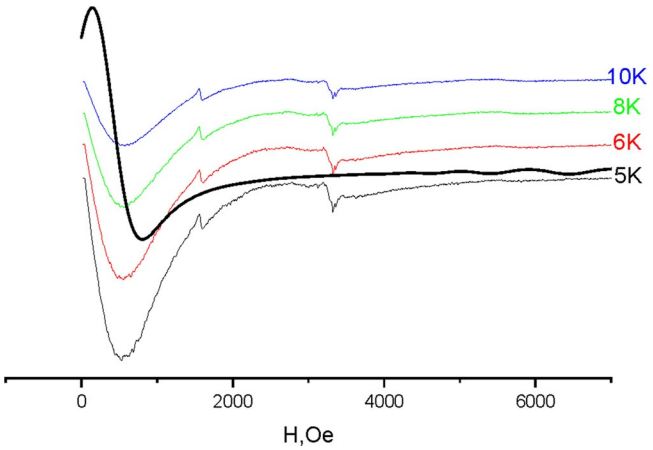

Figure 15. Experimental and simulated (thick line) X-band EPR spectra of **1** ($\nu = 9.399$ GHz).

$g_z = 14.5$ (see Figure S10). This discrepancy cannot be understood on the basis of structural reasons, because all the compounds are isostructural with the isogeometrical core Dy_2Fe_2, and ab initio calculations predict accordingly similar values of g_z for all complexes. Furthermore, the low-temperature magnetization data for **2** (see Figure S4) are well described with the calculated $g_z \approx 19$. Considering that M depends linearly on the g factor, the EPR-extracted $g_z = 14.5$ would not reproduce the experimental magnetization data, which are on the other hand well described by ab initio calculations.

Conclusions

In this work we have investigated the magnetic and SMM properties of a series of $[Fe_2Dy_2(OH)_2(teaH)_2(RC_6H_4COO)_6]$ compounds, in which $teaH_3$ = triethanolamine and R = *meta*-CN (**1**), *para*-CN (**2**), *meta*-CH_3 (**3**), *para*-NO_2 (**4**), and *para*-CH_3 (**5**), by means of detailed ab initio calculations and EPR measurements. The magneto-structural analysis has shown that the exchange coupling parameters for the Fe–Fe pair increase with the Fe-O-Fe angle and Fe–Fe distance. On the other hand, the Dy–Fe coupling decreases with increasing Dy-O-Fe angle and Dy–Fe distance. It was found from BS-DFT calculations that the Fe–Fe interaction in all compounds is much stronger than the Dy–Fe and Dy–Dy interactions, further confirmed by simulations of the magnetic susceptibility data. It was also shown that an account of the exchange interaction of the iron ions is indispensable for a correct description of the energy gap between the two lowest exchange doublets. The dipolar and exchange interactions between dysprosium centers in all the compounds are rather weak. This explains the resulting small separation of the lowest two exchange doublets, supported also by EPR spectroscopy. This small gap enables the relaxation of magnetization to proceed by a spin flip on individual dysprosium ions. Given that both doublets are almost completely populated in the investigated temperature range, it appears to not be surprising that the compounds demonstrate poor SMM behavior. This is because at temperatures exceeding several times the Dy–Dy exchange/dipolar splitting, the latter is no

longer operative, so the blockage of magnetization originates only at individual uncoupled dysprosium ions. However, the transversal components of the ***g*** tensors of the ground Kramers doublets of the dysprosium ions are relatively large (see Table 1), thus allowing unquenched quantum tunneling of magnetization, which impedes the occurrence of magnetization blockage.

Acknowledgements

V.V. acknowledges the postdoctoral fellowships from the Fonds Wetenschappelijk Onderzoek-Vlaanderen (FWO, Flemish Science Foundation). A.S. and V.V. acknowledge the Program of the Presidium of RAS (no. 5). A.B., C.E.A and A.K.P. thank the German Research Foundation, DFG for financial support within the collaborative research center SFB/TRR88 "3MET".

Conflict of interest

The authors declare no conflict of interest. The authors declare no competing financial interest.

Keywords: ab initio calculations · dysprosium · EPR spectroscopy · exchange interactions · iron · magnetic properties

[1] R. Sessoli, D. Gatteschi, A. Caneschi, M. A. Novak, *Nature* **1993**, *365*, 141 – 143.
[2] G. Aromí, D. Aguilà, P. Gamez, F. Luis, O. Roubeau, *Chem. Soc. Rev.* **2012**, *41*, 537 – 546.
[3] M. N. Leuenberger, D. Loss, *Nature* **2001**, *410*, 789 – 793.
[4] G. A. Timco, S. Carretta, F. Troiani, F. Tuna, R. J. Pritchard, C. A. Muryn, E. J. L. McInnes, A. Ghirri, A. Candini, P. Santini, G. Amoretti, M. Affronte, R. E. P. Winpenny, *Nat. Nanotechnol.* **2009**, *4*, 173 – 178.
[5] F. Troiani, M. Affronte, *Chem. Soc. Rev.* **2011**, *40*, 3119 – 3129.
[6] J. D. Rinehart, M. Fang, W. J. Evans, J. R. Long, *J. Am. Chem. Soc.* **2011**, *133*, 14236 – 14239.
[7] F. Liu, D. S. Krylov, L. Spree, S. M. Avdoshenko, N. A. Samoylova, M. Rosenkranz, A. Kostanyan, T. Greber, A. U. B. Wolter, B. Büchner, A. A Popov, *Nat. Commun.* **2017**, *8*, 16098.
[8] S. Demir, M. I. Gonzalez, L. E. Darago, W. J. Evans, J. R. Long, *Nat. Commun.* **2017**, *8*, 2144.
[9] L. Ungur, M. Thewissen, J.-P. Costes, W. Wernsdorfer, L. F. Chibotaru, *Inorg. Chem.* **2013**, *52*, 6328 – 6337.
[10] S. K. Langley, D. P. Wielechowski, V. Vieru, N. F. Chilton, B. Moubaraki, B. F. Abrahams, L. F. Chibotaru, K. S. Murray, *Angew. Chem. Int. Ed.* **2013**, *52*, 12014 – 12019; *Angew. Chem.* **2013**, *125*, 12236 – 12241.
[11] V. Vieru, T. D. Pasatoiu, L. Ungur, E. Suturina, A. M. Madalan, C. Duhayon, J.-P. Sutter, M. Andruh, L. F. Chibotaru, *Inorg. Chem.* **2016**, *55*, 12158 – 12171.
[12] L. F. Chibotaru in *Molecular Nanomagnets and Related Phenomena* (Ed.: S. Gao), **2015**, p. 185.
[13] H. L. C. Feltham, Y. Lan, F. Klöwer, L. Ungur, L. F. Chibotaru, A. K. Powell, S. Brooker, *Chem. Eur. J.* **2011**, *17*, 4362 – 4365.
[14] V. Mereacre, A. Baniodeh, C. E. Anson, A. K. Powell, *J. Am. Chem. Soc.* **2011**, *133*, 15335 – 15337.
[15] A. Baniodeh, V. Mereacre, N. Magnani, Y. Lan, J. A. Wolny, V. Schünemann, C. E. Anson, A. K. Powell, *Chem. Commun.* **2013**, *49*, 9666 – 9668.
[16] A. Baniodeh, Y. Lan, G. Novitchi, V. Mereacre, A. Sukhanov, M. Ferbinteanu, V. Voronkova, C. E. Anson, A. K. Powell, *Dalton Trans.* **2013**, *42*, 8926 – 8938.
[17] M. E. Lines, *J. Chem. Phys.* **1971**, *55*, 2977 – 2984.
[18] L. Ungur, L. F. Chibotaru in *Lanthanides and Actinides in Molecular Magnetism* (Eds.: R. A. Layfield, M. Murugesu), Wiley, Weinheim, Germany, **2015**, pp. 153 – 184.
[19] F. Aquilante, J. Autschbach, R. K. Carlson, L. F. Chibotaru, M. G. Delcey, L. De Vico, I. Fdez Galván, N. Ferré, L. M. Frutos, L. Gagliardi, M. Garavelli, A. Giussani, C. E. Hoyer, G. Li Manni, H. Lischka, D. Ma, P. Åke Malmqvist, T. Müller, A. Nenov, M. Olivucci, T. B. Pedersen, D. Peng, F. Plasser, B. Pritchard, M. Reiher, I. Rivalta, Igor Schapiro, J. Segarra-Martí, M. Stenrup, D. G. Truhlar, L. Ungur, A. Valentini, S. Vancoillie, V. Veryazov, V. P. Vysotskiy, O. Weingart, F. Zapata, R. Lindh, *J. Comput. Chem.* **2016**, *37*, 506 – 541.
[20] L. F. Chibotaru, L. Ungur, *J. Chem. Phys.* **2012**, *137*, 064112.
[21] B. O. Roos, P. R. Taylor, P. E. M. Siegbahn, *Chem. Phys.* **1980**, *48*, 157 – 173.
[22] P. Å. Malmqvist, B. O. Roos, B. Schimmelpfennig, *Chem. Phys. Lett.* **2002**, *357*, 230 – 240.
[23] "SINGLE ANISO," can be found under http://molcas.org/documentation/manual/.
[24] L. F. Chibotaru, L. Ungur, C. Aronica, H. Elmoll, G. Pilet, D. Luneau, *J. Am. Chem. Soc.* **2008**, *130*, 12445 – 12455.
[25] F. Neese, *WIREs Comput. Mol. Sci.* **2012**, *2*, 73 – 78.
[26] F. Neese, *J. Phys. Chem. Solids* **2004**, *65*, 781 – 785.
[27] D. A. Pantazis, X.-Y. Chen, C. R. Landis, F. Neese, *J. Chem. Theory Comput.* **2008**, *4*, 908 – 919.
[28] D. A. Pantazis, F. Neese, *J. Chem. Theory Comput.* **2009**, *5*, 2229 – 2238.
[29] H. A. Kramers, *Proc. Amsterdam Acad.* **1930**, *33*, 959.
[30] M. Shoji, K. Koizumi, Y. Kitagawa, T. Kawakami, S. Yamanaka, M. Okumura, K. Yamaguchi, *Chem. Phys. Lett.* **2006**, *432*, 343 – 347.
[31] K. Yamaguchi, Y. Takahara, T. Fueno, *Applied Quantum Chemistry* **1986**.
[32] V. Vieru, L. Ungur, L. F. Chibotaru, *J. Phys. Chem. Lett.* **2013**, *4*, 3565 – 3569.
[33] C. Cañada-Vilalta, T. A. O'Brien, E. K. Brechin, M. Pink, E. R. Davidson, G. Christou, *Inorg. Chem.* **2004**, *43*, 5505 – 5521.
[34] O. Kahn, *Molecular Magnetism*, VCH Publishers, **1993**.
[35] A. Bencini, D. Gatteschi in *Electron Paramagnetic Resonance of Exchange Coupled Systems*, Springer, Berlin, Heidelberg, **1990**.
[36] I. Dzyaloshinsky, *J. Phys. Chem. Solids* **1958**, *4*, 241 – 255.
[37] T. Moriya, *Phys. Rev.* **1960**, *120*, 91 – 98.
[38] L. F. Chibotaru, N. Iwahara, *New J. Phys.* **2015**, *17*, 103028.
[39] S. Stoll, A. Schweiger, *J. Magn. Reson.* **2006**, *178*, 42 – 55.

Manuscript received: July 26, 2018
Accepted manuscript online: August 14, 2018
Version of record online: October 17, 2018

